Nanocobalt based (Co@Co(OH)$_2$) sand nanocomposite applied to manganese extraction from contaminated water

Rohit Kumar [a], Protima Rauwel [a], Mait Kriipsalu [a], David Wragg [b,c], Erwan Rauwel [a,*]

[a] Inst. of Forestry and Engineering, Estonian Univ. of Life Sciences, Tartu, Estonia
[b] Department of Chemistry, University of Oslo, Oslo, Norway
[c] Institute for Energy Technology, Kjeller, Norway

ARTICLE INFO

ABSTRACT

This study presents the adsorption capability of a filter composed of sand coated with cobalt nanomaterials (CoNM) for the extraction of manganese ions from aqueous media. The study was performed in both batch and dynamic modes in order to evaluate the adsorption capabilities of free-standing CoNM and CoNM-coated sand. The Langmuir and Freundlich isotherm models were applied to the adsorption of manganese ions in batch-mode. The Langmuir model estimated a maximum adsorption capacity of 17.86 mg/g corresponding to a single layer adsorption. Nevertheless, the Freundlich model also characterized the adsorption with a high coefficient of determination, suggesting a multilayered adsorption mechanism of Mn on CoNM. Dynamic mode studies were conducted with different influent Mn concentrations, pH and in the presence of foreign or competing ions (Fe^{3+}, As^{3+}, As^{5+} and Cu^{2+}). The experimental data was fitted with linearized Thomas and Yoon-Nelson models in order to determine adsorption capacities. The multilayered adsorption mechanism was confirmed owing to a high adsorption capacity of 3360 mg/g of active nanomaterials at pH = 6.

1. Introduction

A continuous increase in the discharge of untreated effluent from various industries and through natural processes such as mining, landfill leaching, rock corrosion and soil weathering has resulted in a significant elevation in toxic heavy-metal concentrations in fresh water [1]. In particular, mining effluent comprises of diverse chemical entities, including an upraised amount of iron (Fe), manganese (Mn) [2], and radioactive elements [3]. Among them, Mn is the most difficult to extract because its removal depends on various parameters such as the pH, oxidation state, and presence of other minerals in the aqueous medium. In addition, Mn exists in more than five different oxidation states, out of which Mn^{2+} and Mn^{3+} are mostly encountered in environmental samples in the form of oxides (MnO_2 or Mn_3O_4) [4]. Even though manganese acts as a cofactor for various enzymes and is an essential component for maintaining the functionality and development of the nervous system, its overexposure tends to be toxic for organisms [5]. According to the United States Environmental Protection Agency (USEPA), secondary maximum contamination limit (SMCL) for Mn in drinking water is 0.05 mg/L [6]. Recently, the environmental protection agency (EPA) has placed manganese in the Fourth Draft Contaminant

Candidate List (CCL$_4$) [7]. The presence of Mn ions can negatively affect the aesthetic water quality, raise operational complexity and be harmful for humans. Therefore, it is relevant to develop a cost-effective, efficient and sustainable technology to remove manganese and reduce its concentration to permissible limits. To date, various physical/chemical processes viz. precipitation [8], coagulation/flocculation [9], ion-exchange [10], biological [11–14], and electrochemical technologies [15] are considered and studied for manganese removal from the contaminated groundwater. However, these technologies are energy intensive, costly or require a post-treatment of generated sludge, which therefore restricts their large-scale application. In that regard, adsorption processes offer simpler manipulation and higher efficiencies. Therefore, different kinds of nanoadsorbents for the removal of metallic ions are now gaining ground [16–20]. In a study carried by Muliwa et al., chitosan/bentonite/MnO composite beads were used as an adsorbent material for the removal of Mn^{2+} ions from water with an adsorption capacity of 6 mg/g [3]. It was also reusable after regeneration via HNO$_3$ treatment, highlighting the sustainability of the process. Similarly, Chowdhury et al., observed an effective removal of Mn^{2+} ions using *Mangostana garcinia* Peel-Based Granular-Activated Carbon as an adsorbent and regeneration was done using nitric acid [21]. Various

activated carbon-based and biological sorbents are investigated for divalent-manganese ion removal but their recyclability, along with the use of harsh chemicals for their regeneration are major drawbacks [22–24]. In this context, magnetic adsorbents are seen as good candidates for the extraction of heavy metals because the sorbate can be recovered through the application of an external magnetic field [25]. For instance, Yan and coworkers used magnetic graphene oxide nanoparticles for the removal of Mn^{2+} and Fe^{2+} ions from the micro-polluted water, via a monolayer adsorption mechanism [16]. Even though the recyclability and reuse of these nanoparticles were easily achievable, the degradation of the graphene-oxide support remained nevertheless a concern. To overcome these limitations, magnetic extraction using metallic adsorbents appears to be a viable method. However, pure metal-based adsorbents have not yet been systematically explored owing to their possible oxidation in aqueous medium and in turn, hindering their reusability. Since ion exchange is one of the primary adsorption mechanisms in magnetic nanoparticles, the release of sorbent ions requires secondary adsorption processes for metal-ion capture. To the best of our knowledge, there is no study available describing the use of superparamagnetic cobalt nanoparticles (CoNP) or cobalt coated sand (mCCS) as adsorbents for extracting heavy metal ions, or in particular Mn ions from water. The superparamagnetic cobalt nanoparticles investigated in this study are unique due to their high stability under air and in aqueous medium despite being surfactant-free. Their surfaces are covered by a protective layer of hydroxyl groups, giving them their high stability. This property makes them highly suitable in nanomedicine applications, as assessed in a recent study [26]. The presence of hydroxyl groups would also allow them to interact with other ions present in aqueous media, similarly to layered double hydroxides nanomaterials used for water remediation [27]. The goal of the present study is to assess the adsorption capacity of heavy metal ion pollutants on the surface of CoNP, and compare with the adsorption that takes place on the surface of layered double hydroxides nanomaterials, in which we can observe the adsorption of only one monolayer of heavy metal ions. When CoNP are grown on the surface of a solid support (i.e., sand grains), it increases the available surface of CoNP, which enhances the possibility of chemical interactions with the aqueous medium. Currently, there is no study that describes the possible use of such nanomaterials and nanocomposites for water purification, and more particularly for manganese ion-extraction. Therefore, this study is the first to elucidate the adsorption behavior of CCS towards manganese-ion extraction in both, batch and dynamic modes. The adsorption behavior was examined through breakthrough curves with a fixed bed height and under different parameters such as initial Mn concentration, pH, and competing ions (CI). According to many studies, the presence of iron in water affects the adsorption of Mn, and in Estonia groundwater is known to contain both Mn and Fe contaminants [28]. Reports have also highlighted the presence of arsenic ions in boreholes in Estonia. Therefore, understanding the competing behaviors of these three ions on their simultaneous extraction is the essence of this study. Copper ion was also selected due to its regular presence in wastewater. Langmuir and Freundlich isotherms were applied to batch-mode adsorption and the breakthrough curves of the dynamic mode adsorption were analyzed using Thomas and Yoon-Nelson models. If not stated otherwise, all the experiments were performed with Mn^{7+} as an adsorbate. Therefore, our study showed a novel and sustainable alternative to treat heavy metal-contaminated water even in the presence of competing contaminants.

2. Experimental section

2.1. Chemicals

All the chemicals i.e. Potassium permanganate ($KMnO_4$), Hydrochloric acid (35% HCl, Lach:ner), Sodium Hydroxide (NaOH, Lach:ner), copper nitrate (99%, Arcos organics), Ferric chloride, sodium arsenate

dibasic heptahydrate (98%, Alfa Aesar), arsenic trioxide (99.5%, Alfa Aesar), Ascorbic acid, Alkaline cyanide solution, PAN indicator used were of analytical grade. De-ionized water was used for all the solution preparations.

2.2. Materials

The superparamagnetic cobalt nanoparticles (CoNP) were provided by PRO-1 NANOSolutions Pvt. Ltd. (http://www.pro1nanosolutions.eu/). A recent report highlighted that superparamagnetic metal Co nanoparticles are coated by a monolayer of hydroxyl groups ($Co(OH)_2$)[29], rendering them non-pyrophoric and ultra-stable in air. Moreover, the Co metal nanoparticles are of high purity with less than 0.9%wt. of carbon [15]. The sand coated with superparamagnetic cobalt nanoparticles (CCS) with a Co NP/sand weight ratio of 1:1111 (0.09%wt.) was also provided by PRO-1 NANOSolutions Pvt. Ltd.

2.3. Characterizations

The Mn concentration was measured with a Lovibond water testing kit (Method-Vario PP LR) having a detection range of 0.01–0.7 mg/L. Scanning electron microscopy (SEM) images were recorded using EVO LS15 Zeiss in secondary electrons mode. Samples were studied without any carbon or gold coating, simply by depositing some powder onto a carbon gluing tape. X-ray diffraction (XRD) patterns were collected in Bragg–Brentano geometry using a Bruker D8 Discover diffractometer (Bruker AXS, Germany) with Cu $K_{\alpha 1}$ radiation ($\lambda = 0.15406$ nm) selected by a Ge(111) monochromator. A LynxEye detector was used in fluorescence suppression mode. High-resolution transmission electron microscopy (HRTEM) was carried out on 80–300 FEI Titan, operating at 300 kV, disposing a point-to-point resolution of 1.4 Å. Both, the Co NP and CCS were characterized by Fourier transform infrared (FTIR) spectroscopy Fourier-transform infrared spectroscopy (FTIR) (Thermo Scientific Nicolet is10). High-resolution computed X-ray tomography (XRT) was carried out on a YXLON FF35 CT. The manganese ion concentration in water was determined using Manganese LR PP method of Lovibond MD-610 photometer and water testing kit. The wavelength, cuvette length, and detection range were 560 nm, 24 mm, and 0.01–0.7 mg/L, respectively. The method follows the addition of ascorbic acid, alkaline cyanide solution and a PAN indicator solution in water and testing the sample consequently via a colorimetric technique.

2.4. Batch adsorption

Batch experiments were performed by adding 10 mg of pure cobalt nanoparticles in different manganese concentrated solutions ranging from 0.5 to 100 mg/Lin cylindrical centrifuge tubes of 15 mL. In order to obtain the equilibrium saturation time of the adsorbent, an initial Mn concentration of 50 mg/L was used, and Mn concentration was measured after fixed time intervals. This saturation time was used to calculate the time dependent concentration of Mn for each concentration. The adsorption capacities (q_e, mg/g) were calculated using the equation:

$$qe = \frac{(Co - Ct).V}{m} \tag{1}$$

Where, C_o and C_t represent initial and time specific concentration, V is the volume filtered in L, and m is the amount of adsorbent in g.

Adsorption isotherm models describe the metal-ion distribution in the liquid phase adsorbed on the free-standing cobalt nanoparticles. The experimental results were then fitted with Langmuir and Freundlich linear regression models to elucidate the adsorption patterns (Eqs. S1–S3).

2.5. Dynamic mode studies

The continuous fixed-bed adsorption column or the filter consisted of 7.8 g of sand coated with superparamagnetic cobalt nanoparticles with a specific surface of 25.272 $cm^2.g^{-1}$ (Fig. S1) in a cylindrical centrifuge tube (15 mL). The mass of sand corresponds to an active surface of 197.12 cm^2. An aeration pump (AQUEAL PAT mini) injected contaminated water continuously into the filter. The adsorption begins from the uppermost part of the column and the maximum adsorption zone starts migrating towards the bottom of the column. Two parameters were monitored carefully i.e., the breakthrough point and the exhaustion point. When the effluent concentration reaches 0.1% of the initial concentration, it is referred to as the breakthrough point. Similarly, when the effluent concentration reaches 90–95% of the initial concentration, it is referred to as the exhaustion point on the breakthrough curve[30].

The performance of the column is expressed in terms of breakthrough curves, a plot of C_t/C_0 vs time (t), where C_t represents Mn concentration after each time interval and C_0 is the initial Mn concentration. The adsorption experiments were performed under a continuous dynamic flow of $KMnO_4$ aqueous solution and the breakthrough behavior was studied for initial Mn concentrations of 30, 50 and 85 mg/L~~ppm~~; the influence of pH was studied for different values (4, 7, 9, and 12) that were adjusted with NaOH and HCl accordingly, and the influence of foreign competing ions (Fe^{3+}, As^{3+}, As^{5+} and Cu^{2+}) was also investigated for a Mn concentration of 85 mg/L. All the experiments were performed with a constant bed mass of 7.8 g, an average flow rate of about 3.5 mL/min and effluent concentration was measured using

Lovibond MD 610 and water testing kit at fixed intervals of 10 min.

The total adsorption (q, mg) was calculated as:

$$q = \frac{Q}{1000} \int_{t(initial)}^{t(total)} C_{ad}.dt \tag{2}$$

Where Q is the flow rate (mL/min) and $C_{ad} = C_i - C_t$, is the total adsorbed concentration (mg/L) of manganese. In fact, for a given bed mass (m), the equilibrium adsorption capacity (q_e, mg/g) can be calculated as:

$$qe = \frac{q}{m} \tag{3}$$

To illustrate the adsorption studies, adsorption models, such as Thomas model and Yoon-Nelson model, were applied to the dynamic flow experimental data, in this study (Eqs. S4–S6).

3. Results and discussion

3.1. Characterization of CoNP

X-ray diffraction shows that the nanoparticles are crystalline and contain both cubic and hexagonal cobalt (Fig. 1(a))[31]'[32]. In some cases, purely cubic phases were obtained (see Fig. S2). The HRTEM micrograph of Fig. 1b provides an overview of the studied CoNP, highlights that they are crystalline and monodispersed with an average diameter of 8–10 nm[26]. SEM study shows that before being used of Mn ions extraction, the free-standing CoNP are agglomerated into larger particles of diameters ranging from 100 nm to 2 (Figs. 1a and 1d).
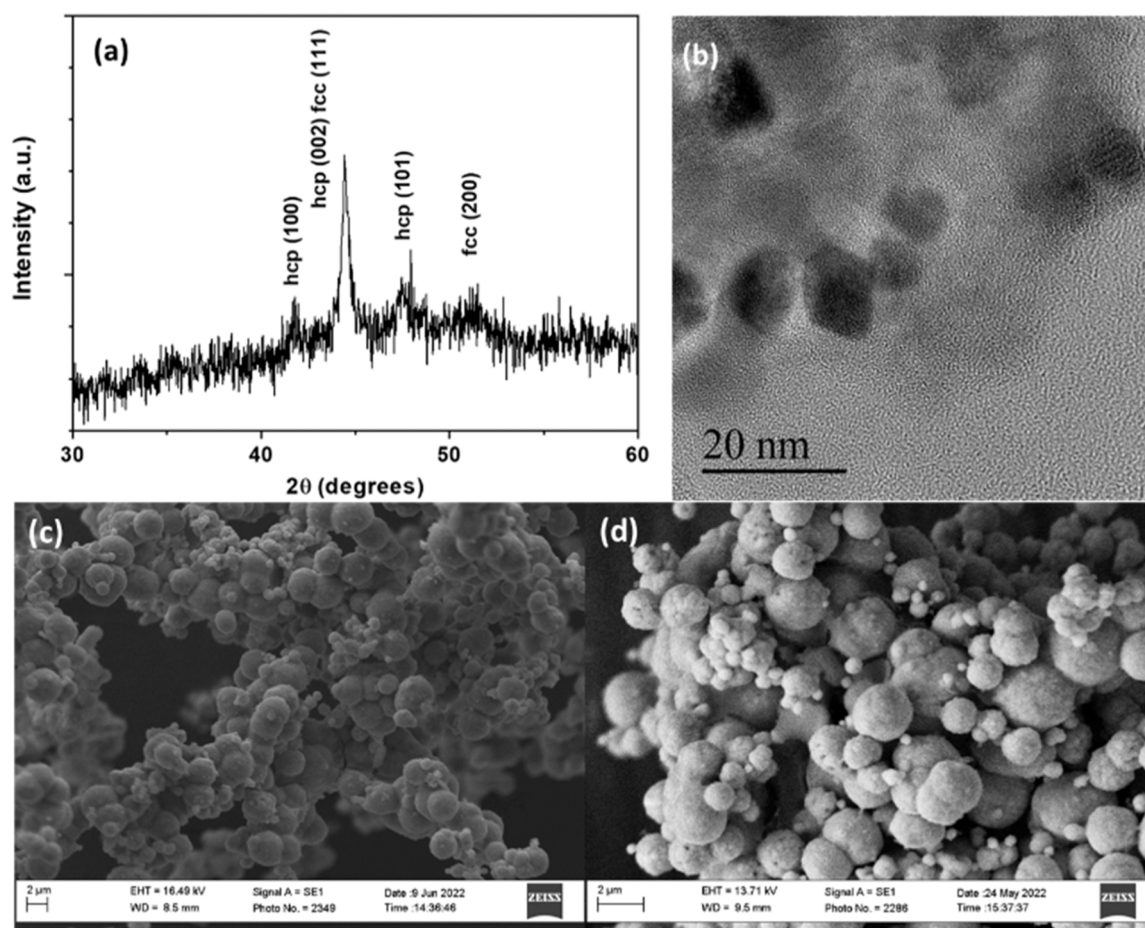
Characterization of CoNP

Fig. 1. (a) X-Ray diffraction patterns of the Co metal nanoparticles, (b) TEM images of free-standing CoNP, (c) and (d) SEM images of agglomerated free-standing CoNP.

3.2. Batch studies

Magnetic extraction experiments were first performed to assess the extraction capacity of the freestanding CoNP, using their intrinsic superparamagnetic properties [26]. For equilibrium studies, an aqueous solution containing 0.5–100 mg/L initial Mn concentration and 10 mg of freestanding CoNP as an adsorbent were used. Since, adsorbent-adsorbate contact time plays a crucial role in the adsorption process; the removal efficiency of the NP was therefore controlled at different time intervals. In Fig. 2a, the effect of contact time in the batch removal process of manganese ions for a concentration of 50 mg/L reaches an equilibrium plateau at 5 min of adsorption. Therefore, the parameters, such as the adsorption capacities (q_e, mg/g) and the effluent Mn concentration (C_e) were estimated at the saturation time of 5 min.

The adsorption behavior can be explained as a 2-step mechanism. Initially, the availability of active sites on the surface of CoNP promotes the fast adsorption and in the second phase, the adsorption attains an equilibrium due to the exhaustion of active sites, which results in slower adsorption thereafter. The equilibrium studies for the Mn removal were extensively investigated through the linear plots of Langmuir and Freundlich adsorption models. A linear plot of C_e/q_e versus C_e representing the Langmuir adsorption model (Fig. 2b) provided parameters, such as the maximum adsorption capacity (q_m) and energy of adsorption that is considered as the same for all sites or a homogenous adsorption process. Similarly, the plot of $\ln(q_e)$ versus $\ln(C_e)$ determined the Freundlich constant (K_f) and the adsorption intensity (n) (Fig. 2c). The calculated parameters for both the models are presented in Table 1.

The adsorption isotherm shows a good fit with both, Langmuir and Freundlich models, supporting both monolayer and multilayered adsorption of manganese ions onto the surface of CoNP. In fact, the multilayered adsorption was more favorable, suggesting the efficiency of cobalt NP in continuous growth of Mn ions over its surface. The maximum adsorption capacity (q_m) was 17.86 mg/g of pure CoNP. The adsorption intensity (n) value of 1.61 (>1) corresponds to the occurrence of physical adsorption processes at the interface of Co and Mn ions. In order to examine the propensity of the CoNP surface towards adsorbing Mn ions, the separation factor (R_L) was also determined for concentrations ranging from 0.5 to 100 mg/L through the formula:

$$R_L = 1/ (1+b \cdot C_o) \tag{4}$$

Measured R_L values range from 0.973 to 0.152 (i.e., $0 < R_L < 1$), indicating the favorable disposition of the CoNP surface for all the Mn concentrations. In this study, given that CoNP are agglomerated in solution, the available surface of interaction with the liquid medium (i.e., contaminated water) is therefore limited to the surface of the agglomerate. Since agglomerated nanoparticles can be considered as surfaces with high roughness, the Langmuir isotherm that usually applies to flat surfaces, involves simultaneous adsorption and desorption, may not be

Table 1
Langmuir and Freundlich parameters.

Langmuir	b (L/mg)		q_m (mg/g)	R^2
	0.071		17.86	0.98
Freundlich	**K_f ((mg/g) (L/mg)$^{1/n}$)**		**n**	**R^2**
	1.58		1.61	0.99

the most adapted in the present case. Rough surfaces have a higher specific surface than flat surfaces with the same surface area. In principle, the adsorption capacity of the latter is higher. It is therefore difficult to rely on Langmuir isotherm adsorption characteristics in order to assess accurately the maximum adsorption capacity (q_m) in the present case, as it may be underestimated. In addition, since the agglomeration of nanoparticles due to their superparamagnetic properties is inevitable, therefore the nanoparticles below the surface of the agglomerate do not participate in the adsorption process. To circumvent the phenomenon of CoNP agglomeration, Co nanomaterials were directly grown in-situ on the surface of a support material, such as sand that is widely used in water treatment processes.

3.3. Characterization of Co NP after extraction

Physical and chemical characterization of the CoNP after extraction of Mn ions from the contaminated water samples highlighted the adsorption mechanism. The XRD pattern after batch test extraction shows 3 phases (Fig. 3). The crystalline face-centered cubic i.e., Fm3m phase of CoNP with diffraction peaks at $<111>$, $<200>$ and $<220>$ is still present, along with a secondary phase of hexagonal CoNP ([100] and [101]) peaks, COD 9008492). At $2\Theta = \sim59°$ a peak is visible which is attributed to the $<220>$ reflection of MnO manganosite (COD 9006659). SEM analyses performed on CoNP after extraction of Mn ions from contaminated solutions confirm the presence of Mn on the surface of CoNP during the extraction process.

After extraction, SEM study highlights that all CoNP have a 'spiked' or 'platelet' like appearance (Fig. 3b) confirming the growth of the MnO phase that was evaluated by XRD. Furthermore, XRD study suggests that manganese oxide is mainly amorphous, but also contains MnO crystallites. The higher magnification image of Fig. 3c gives an idea of the morphology of the amorphous MnO coating consisting of nano/micro sheets or microflower arrangements fully covering the CoNP. The clear change in the morphology of the CoNP indicates and the formation of hierarchical structures confirms that the Mn adsorption is a superficial and physical adsorption process. The SEM study shows that Mn ions are extracted in solid form on to the surface of agglomerated CoNP and is clearly not a monolayer adsorption (Langmuir adsorption) process, considering the micrometric growth of the sheets. This magnetic extraction process should also enable the future reclamation of metallic
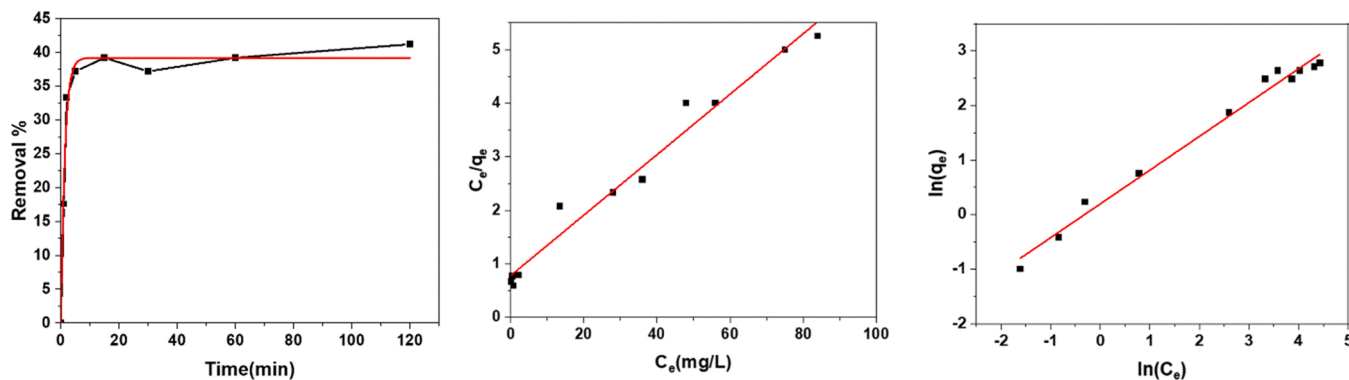

Fig. 2. (a) Effect of contact time on the removal of manganese ions ([Mn]=50 mg/L, T = 25°C, V=10 mL, m_{CoNP} =10 mg); Adsorption isotherms linear fitting for (b) Langmuir and (c) Freundlich model of manganese removal in batch-mode (initial Mn conc.= 0.5–100 mg/L, T = 25°C, V=10 mL, m_{CoNP} =10 mg).
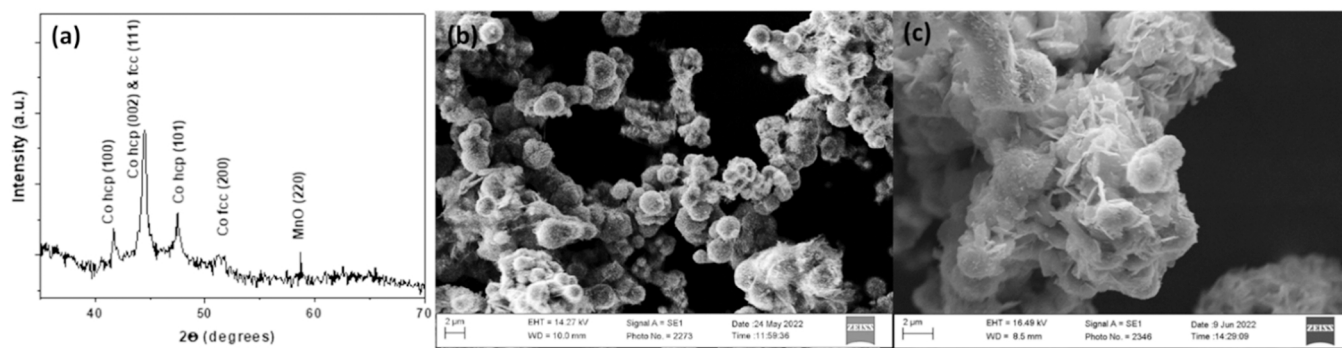
Fig. 3. (a) XRD patterns of CoNP after the extraction of Mn ions, (b) and (c) SEM images of agglomerated CoNP covered by manganese oxide coating after extraction on Mn ions.

ions that are converted into solid metal oxide upon extraction.

3.4. Continuous adsorption studies

The batch-mode adsorption studies mentioned above are usually limited to smaller volumes of contaminated water. However, in continuous-flow mode, the adsorption capacity also depends on the fluid mechanics. Therefore, batch-mode studies are appropriate to establish a proof-of-concept but provides insufficient data for the scale-up of the adsorption process. In addition, the agglomeration of the nanoparticles in batch-mode reduces the effective surface of the nanoparticles and in turn, the overall efficiency of the adsorption process. This tendency is even more pronounced when working with large-volume industrial effluents, where flow rates as well as contaminant concentrations are variable. The full recovery of the sorbent with a magnetic field in such a scenario could be challenging. Therefore, continuous mode studies provide a brief insight in understanding the influence of flow patterns in order to design a prototype filter for large-scale applications. The flow mode studies were performed under different experimental conditions, such as i) inlet Mn concentration, ii) pH ranging from 4 to 12, and iii) in the presence of foreign ions like Fe^{3+}, As^{3+}, As^{5+} or Cu^{2+}. The adsorption behavior was elucidated with breakthrough curves and based on the parameters calculated using two adsorption models.

The adsorption capacity of CCS was studied with 7.8 g of activated sand corresponding to an active surface of 197.12 cm^2 for three different Mn concentrations of 30, 50, and 85 mg/L at an average flow rate of 5 mL/min at room temperature (25 °C) (Fig. S1). The pH of the solution was measured before filtration with pH values of 7.75, 6.8 and 6.0 for Mn concentrations of 30, 50 and 85 mg/L, respectively. The breakthrough curves representing the adsorption behavior at different concentrations are shown in Fig. 4a. For lower Mn concentrations, the

breakthrough plateau was reached after a longer period. With higher concentrations, a steep increase in the Mn extraction is observed in the first 40 min followed by equilibrium on reaching 95% Mn extraction. For higher concentrations of Mn, breakthrough curves were obtained in more quickly. The results reveal the influence of Mn concentrations in solution on saturation rate and breakthrough time. It is evident from the breakthrough plot that for higher concentrations, there is a decrease in the breakthrough time and an increase in the saturation rate.

This is due to the rapid adsorption of Mn ions on CCS in high amounts, leading to an expeditious occupation of the binding sites on the surface of activated sand. However, a reverse trend was observed for lower concentrations corresponding to the slower mass transfer rate, which in turn results in a longer saturation time. In addition, we observed a complete adsorption (below detection limit) of Mn ions for an initial concentration of 30 mg/L within the first 10 min. Such adsorption highlights the high adsorption capacity of the Co nanomaterials when anchored on a support like sand. For this reason, the fitting of the breakthrough curve is more complex ($R^2 = 0.95$) for lower concentrations of 30 mg/L. The data was fitted using Thomas and Yoon-Nelson models, and all the adsorption parameters are listed in Table 2.

Table 2
Adsorption parameters for different initial Mn concentrations.

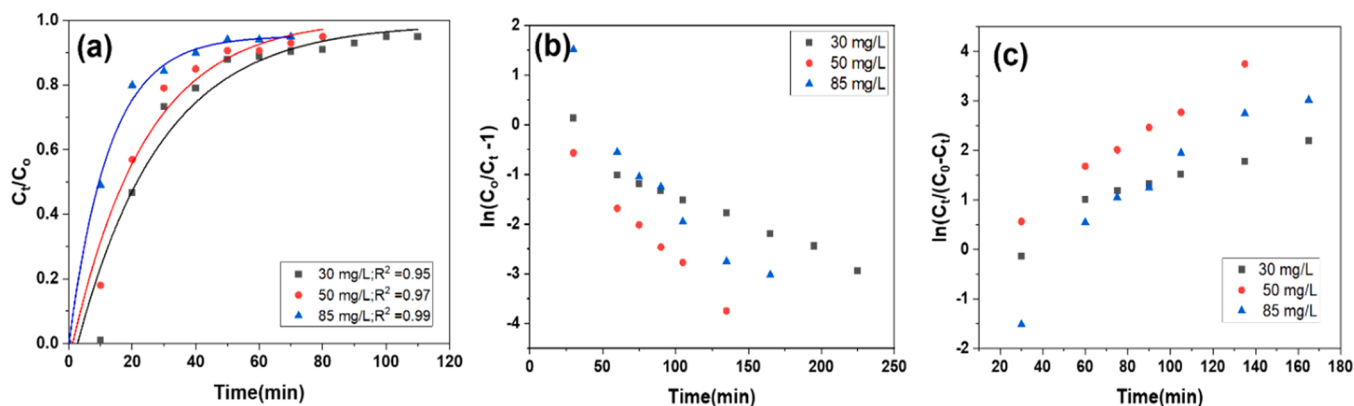| Mn conc. (mg/L)	Thomas			Yoon-Nelson		
	K_{TH} (mL / min.mg)	q_e (mg/ g)	R^2	K_{YN} (min^{-1})	Ʈ (min)	R^2
30	1.0	0.247	0.94	0.015	54	0.91
50	0.268	0.526	0.99	0.03	10.66	0.99
85	0.376	3.025	0.91	0.032	7.33	0.91

Fig. 4. (a) Breakthrough curves for influent Mn concentration of 30, 50 and 85 mg/L(with pH = 7.75, 6.8 and 6.0 respectively); linear fitting of (b) Thomas and (c) Yoon-Nelson model for the different initial Mn concentrations (T = 25 °C, V = 1 L, Q = 5 mL/min, m = 7.8 g of mCCS).

For the Thomas model, the regression coefficient (R^2) was found to be 0.94, 0.99, and 0.91 for 30, 50, and 85 mg/L initial Mn concentrations respectively (Fig. 4b). The adsorption capacity (qe, mg/g of CCS) of the coated sand was calculated from the intercept of the curve and was found to be $\sim$ 0.247 mg/g, 0.526 mg/g, and 3.025 mg/g for 30, 50, and 85 mg/L initial Mn concentrations, respectively. Since, the coated sand consists of 0.09% CoNP, the adsorption capacity should therefore be multiplied by a factor of 1111 in order to obtain the appropriate values with respect to CoNP only, as it is the active material. The calculations result in an adsorption capacity of CoNP of 274.4 mg/g, 584.5 mg/g, 3360.3 mg/g for 30, 50, and 85 mg/L Mn concentrations in the contaminated solutions, respectively. For a concentration of 30 mg/L, all Mn ions were extracted from the solution during the first 10 min (below detection limit). However, for higher adsorbate concentrations, the prepared filter could not fully extract the Mn ions, even though it presented a higher extraction over a longer period. This suggests that the sorbent is capable of scavenging the sorbate more efficiently when higher quantities of sorbate are present for the same quantity of sorbent. The theoretical Yoon-Nelson model was applied to investigate the adsorption behavior of Mn ions on the CCS surface. The Yoon parameters (K_{YN} and τ) were determined from the linear regression analysis (Fig. 4c). Experimental results showed that the rate constant K_{YN} increased and τ decreased with the increase in inlet Mn concentration from 30 mg/L to 85 mg/L. On comparing the values of the regression coefficients, the Thomas model clearly fits well with the experimental data for all Mn concentrations. It is therefore an apt model to evaluate the adsorption behavior of Mn ions on CCS.

Exhausted CCS was analyzed in order to confirm the presence of manganese on the surface of the sand. Fig. S3 shows the FTIR spectra of CoNP anchored on sand support, and bonded with manganese ions after adsorption studies. We observed a number of peaks corresponding to different chemical entities. The peak around 541 cm^{-1} represents the Mn-O stretching frequency; Co-O asymmetric stretching is observed around 1398 cm^{-1}. A previous study showed that these Co nanoparticles are coated with a monolayer of hydroxyl groups ($Co(OH)_2$) that could bind with Mn^{2+} or MnO_4^- ions[29]. In addition, a peak at 1170 cm^{-1} corresponds to the stretching vibration peak of silica particles, originating from sand. The FTIR spectra contained clear peaks of a manganese-cobalt complex that is formed during the process of adsorption.

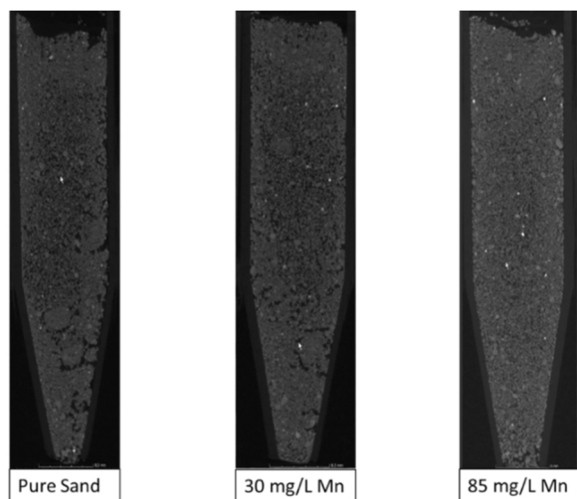The adsorption of Mn ions on the cobalt-coated sand surface was also confirmed using X-ray tomography (XRT) (Fig. 5). The tomography profile displays a 2D view of the target deciphering the surface characteristics of a material. To highlight the adsorption of Mn ions on the surface of the coated sand, and to evaluate the distribution of the adsorbed Mn along the length of the filter, we performed XRT analysis on three filters. One filter was the as-prepared one before extraction with only CoNP anchored on the sand surface and 2-exhausted filters used for 30 mg/L and 85 mg/L of Mn ion extraction. The breakthrough curves showed an increase in the adsorption capacity with increase of Mn concentration in the solution, which should be detectable in the X-Ray tomograms.

Fig. 5 highlights the presence of adsorbed Mn ions on the surface of activated sand in an exhausted filter (bright spots). The increase in initial Mn concentration showed higher adsorption represented as white dots that are larger and more numerous in the case of the filter used for filtering a solution containing 85 mg/L of Mn ions, with more densely packed grains showing a more uniform distribution. It is evident that when the initial concentration increased from 0 mg/L to 85 mg/L, the granular appearance of the tomograms is more enhanced, and the sand appears brighter on the XRT scan, indicating an increased adsorption on the sand surface. Through XRT is it possible to discriminate the sand grains from the coating. The presence of visible bright spots (Fig. S4) confirms the physical adsorption of Mn in solid form on the surface of the sand, and not as a single monolayer, also corroborating with SEM and XRD studies.

3.5. Influence of pH on continuous adsorption

The pH is one of the important factors that influences the adsorption process of metallic ions onto the surface of the adsorbent, and more particularly with activated sand that is coated with CoNP covered by hydroxyl groups[29]. However, the adsorption capacity of an adsorbent depends also on the speciation of metallic ions and the functional moieties present on their surfaces. The pH was varied from 4 to 12 and the adsorption capacity was calculated using Eq. (6). The breakthrough behavior was analyzed through the breakthrough curves, which is shown in Fig. 6a. The breakthrough time under different pH is similar because the initial concentration remained constant at 85 mg/L.

In order to understand and analyze the adsorption process, the breakthrough curves were fitted with the linear form of the Thomas and Yoon-Nelson model to determine the adsorption parameters (see Figs. 6b and 6c, and Table 3).

The equilibrium adsorption capacities (q_e, mg/g of CCS) were found to be 0.618 mg/g, 1.440 mg/g, 0.877 mg/g, and 0.258 mg/g for pH of 4, 7, 9, and 12 respectively. Therefore, the adsorption capacities of CoNP (multiplied by 1111) are calculated as 687.1 mg/g (pH = 4), 1599.8 mg/g (pH = 7), 974.2 mg/g (pH = 9), and 303.4 mg/g (pH = 12). The core shell of CCS consists of a thin shell of $Co(OH)_2$ which stabilizes the metallic cobalt core and prevents oxidation in air[29]. In the acidic medium (pH = 4), the solution contains an excess of protons (H^+), which leads to a strong interaction with the hydroxyl groups (OH$^-$) present at the surface of cobalt to produce water molecules. This phenomenon reduces the binding receptors (OH$^-$) on the cobalt surface, and thus decreases the adsorption capacity of the adsorbent. However, in a highly basic medium (pH = 12 or more), the solution contains an excess of hydroxyl ions which probably dissolves the cobalt coating on the surface of the activated sand in the form of hydroxides ($Co(OH)_2$) and we observed a release of cobalt in the effluent samples. To confirm this phenomenon, an additional experiment was conducted at pH = 14 which showed much higher release of Co ions into the effluent sample and showed a lower saturation point of the filter when tested in highly alkaline medium. Interestingly, in this study, pH = 7 serves as an optimal condition to get maximum adsorption capacity. However, the first experiment showed that the adsorption capacities at pH = 6 is higher (3360.3 mg/g). Therefore, a pH of 6 appears optimum for the extraction of Mn ions.

Fig. 5. X-ray tomography profiles of the CCS before filtration of water solution containing Mn ions (Pure Sand), exhausted filter after filtration of a solution containing 30 mg/L of $KMnO_4$, and exhausted filter after filtration of a solution containing 85 mg/L of $KMnO_4$.
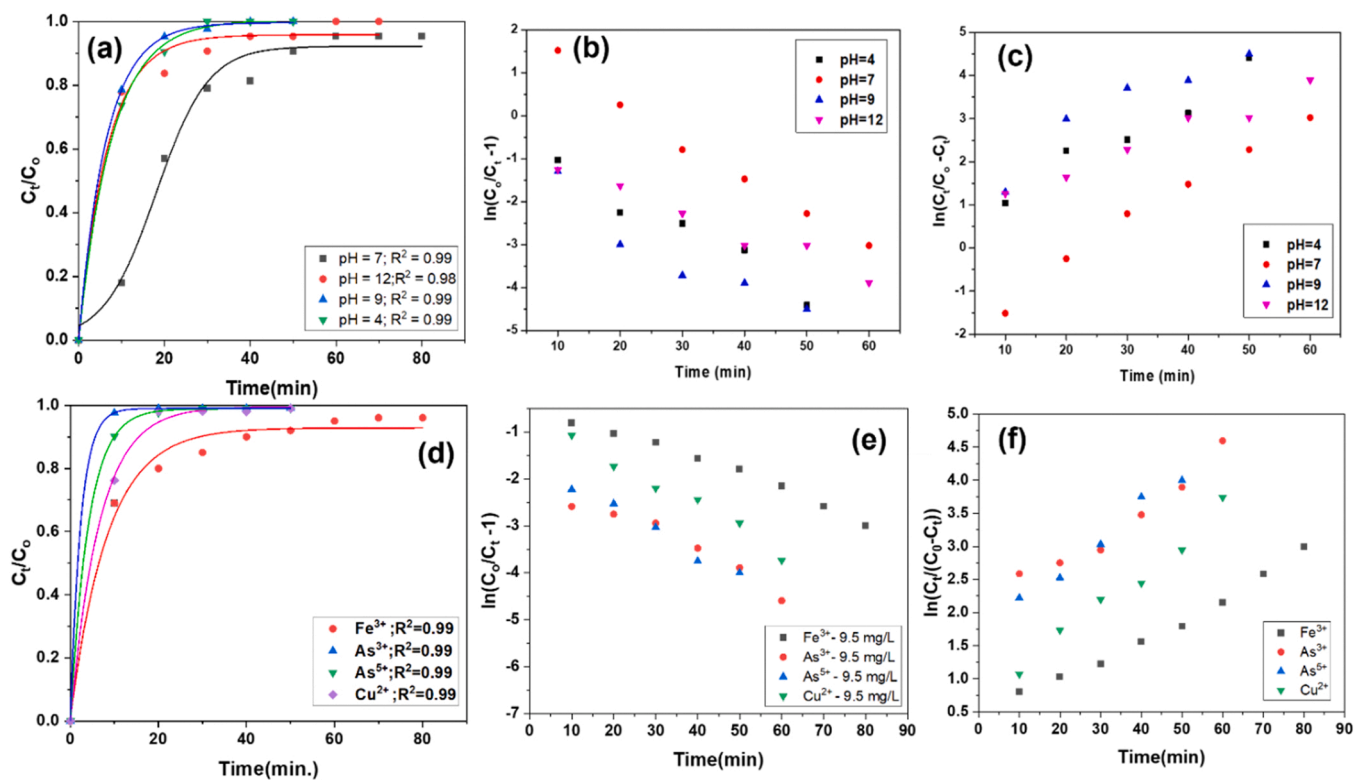
Pure Sand | 30 mg/L Mn | 85 mg/L Mn

Fig. 6. (a) Breakthrough curves for different pH (4, 7, 9, 12); linear fits for (b) Thomas and (c) Yoon-Nelson models for the effect of pH on the extraction efficiency of Mn (T = 25 °C, Q = 5 mL/min, C_0 = 85 mg/L, m = 7.8 g of mCCS), (d) breakthrough curves for different competing ions ([CI] = 9.5 mg/L, Fe^{3+}, As^{3+}, As^{5+}, and Cu^{2+}), C_0 and C_t are the initial concentration and final concentration at time (t) of Mn ions; linear fitting for (e) Thomas (f) Yoon-Nelson fit for the effect of CI on the extraction efficiency of manganese (C_0 = 85 mg/L, [CI] = 9.5 mg/L, T = 25 °C, Q = 5 mL/min, m = 7.8 g mCCS, T = 25°C).

Table 3
Adsorption parameters for different initial pH of the Mn contaminated aqueous media, and different competing ions (Fe^{3+}, As^{3+}, As^{5+}, Cu^{2+}) with [CI] = 9.5 mg/L.

pH	Thomas			Yoon-Nelson		
	K_{TH} (mL / min.mg)	q_e (mg/g of mCCS)	R^2	K_{YN} (min^{-1})	T (min)	R^2
4	0.66	0.618	0.99	0.076	20	0.95
7	0.941	1.440	0.98	0.08	26.5	0.98
9	0.82	0.877	0.96	0.071	5	0.96
12	0.89	0.258	0.95	0.056	5	0.99
ions	Thomas			Yoon-Nelson		
	K_{TH} (mL/min. mg)	q_e (mg/g of mCCS)	R^2	K_{YN} (min^{-1})	T (min)	R^2
Fe^{3+}	0.471	2.68	0.98	0.031	50	0.98
As^{3+}	0.365	0.68	0.94	0.04	12.6	0.94
As^{5+}	0.588	0.65	0.97	0.05	11.93	0.97
Cu^{2+}	0.588	1.82	0.98	0.05	33	0.98

3.6. Influence of competing ions on continuous adsorption

In industrial effluents, a variety of chemical moieties including organic and inorganic elements (i.e., metallic ions) are simultaneously present, making selective extraction challenging. In the Estonian groundwater, heavy metal ions, such as iron and arsenic are present. Zekker et al. found about 4.3 ± 0.1 mg/L of Fe and 0.18 ± 0.004 mg/L Mn in the Estonian water bodies[28]. In addition, As^{3+} and As^{5+} were also found in the Estonian water with a concentration of about 0.025 mg/L which is beyond the permissible limit of 0.01 mg/L. Therefore, the experiments were conducted with iron as one of the competing ions along with arsenic. In order to demonstrate clearly the competition with the foreign ions, the initial concentration of all the foreign ions was set at 9.5 mg/L in order to compare their relative adsorption. The filter performance was evaluated through the breakthrough curves representing the adsorption behaviour in the presence of different competing ions is shown in Fig. 6d.

For this study, we have mixed 9.5 mg/L of Fe^{3+}, As^{3+}, As^{5+}, and Cu^{2+} in an aqueous solution containing an initial concentration of 85 mg/L of $KMnO_4$. In the presence of Fe^{3+}, we observed a longer breakthrough time, which is probably because of the symbiotic behaviour of ferric ions with Mn. This synergistic effect resulted in an increase in the saturation time of Mn ions on the vacant sites of the coated sand. However, we encountered a similarity in the breakthrough time in the presence of As^{3+}, As^{5+} and Cu^{2+} ions, indicating a decrease in adsorption of Mn ions and breakthrough time, visible in Fig. 6d.

For the linear regression of the Thomas model, the regression coefficient values were 0.95, 0.99, 0.99, and 0.99 for Fe^{3+}, As^{3+}, As^{5+}, and Cu^{2+} respectively (Figs. 6e and 6f). The adsorption capacities (per g of mCCS) for Mn ions in the presence of competing ions of Fe^{3+}, Cu^{2+}, As^{3+} and As^{5+} were 2.68 mg/g, 1.82 mg/g, 0.68 mg/g, and 0.65 mg/g, which is lower than for water contaminated with only 85 mg/L of Mn ions (3.025 mg/g). Therefore, the adsorption capacities (per g of CoNP) is 2974.1 mg/g (Fe^{3+}), 2025.4 mg/g (Cu^{2+}), 760.6 mg/g (As^{3+}), and 722.1 mg/g (As^{5+}). In fact, the highest adsorption-capacity of CCS was in the presence of Fe^{3+}, very similar to the adsorption capacity without any competing ions (3360.3 mg/g). It could be attributed to a possible synergistic effect of Fe^{3+} and Mn adsorption. However, in environmental conditions, Fe^{2+} oxidizes to ferric oxide and the additional electron reduces other metallic ions.

In the case of arsenic ions (As^{3+} and As^{5+}), a large decrease in the adsorption capacity was observed which might be due to the different binding mechanisms of the cations, Generally, arsenic adsorption can be specific or non-specific depending on charge transfer from the surface of nanocomposite and through direct ligand exchange. When arsenite is oxidized to arsenate and MnO_2 is reduced to MnO, As^{5+}/Mn^{2+} complex

is formed, which is believed to bind to the adsorbent surface. XRD analysis has also shown the presence of MnO or a Mn^{2+} oxidation state, supporting this mechanism. This process increases the adsorption of Mn ions and therefore we observed a higher adsorption capacity in case of As^{3+} ions than in the case of As^{5+}. Whereas, in presence of As^{5+}, there is no reduction of Mn^{+7} and which results in a decrease in the adsorption capacity compared to As^{3+}.

The combination with arsenic ions probably prevents further growth of manganese oxide on the mCCS surface and decreases the adsorption capacity to 722.1 mg/g of CoNP anchored on mCCS surface. For the Yoon-Nelson linear fitting, we obtained the regression coefficient values of 0.98, 0.94, 0.98, and 0.98 for Fe^{3+}, As^{3+}, As^{5+}, and Cu^{2+} respectively. All the other parameters were determined and are listed in Table 3. On comparing the regression values, both the Thomas and the Yoon-Nelson models showed a good fit with the experimental data and can be applied to model the adsorption process of Mn ions on the surface of CoNP activated sand.

3.7. Comparison with other studies

Manganese ions are known as difficult pollutants to extract from water, and some investigations using other adsorbents were already performed, some including nanomaterials and nanocomposites. In all these studies, authors applied Langmuir and Freundlich models that enables a direct comparison of the adsorption capacity we measured in this study with other values published in recent and older studies (Table 4).

The adsorption capacities found in other studies range from 5.6 to 165.5 mg/g of adsorbent, but the sources of manganese were also different in some of these studies, which may affect also affect the adsorption capacity due to different chemistry involved. In the case of magnetic extraction, a similar adsorption capacity was found with magnetic graphene oxide[16]; 15 mg/g compared to 17.86 mg/g in our study. Similar adsorption capacity was also measured with graphene oxide–ZnO Nano-composites[33] (20 mg/g). It highlights that magnetic extraction and the use of free-standing nanomaterials exhibit a lower efficiency than continuous mode methods. The functionalization of hydrogel[37] or polymer like DMAPAAQ or PSA showed a higher adsorption capacity extraction of 39 and 165 mg/g respectively. The functionalization of sand with cobalt nanomaterials showed a low adsorption capacity (0.247–3.025 mg/g) due to the high weight ratio of sand (i.e., 99.995%), but if we only consider the weight of active

nanomaterials, the adsorption capacity is higher than all former values published till now ranging from 274.4 to 3360.3 mg/g depending on the initial concentration of Mn ions present in the solution.

The superparamagnetic cobalt nanoparticles investigated in this study are covered by a protective layer of hydroxyl groups on their surface rendering them highly stable. The presence of the hydroxyl layer on the surface of CoNP opens the binding sites (oxygen ion) for the adsorption of metal ions carrying positive charges through possible chelation or more stable bonding, comparable to the adsorption that takes place in layered double hydroxide nanomaterials tested for water remediation[27]. This hypothesis is supported by the influence of the pH during the adsorption process that is reduced for high and low pH due to the changes in interaction with the hydroxyl groups present on the surface of the CoNP. However, the adsorption process in the case of layered double hydroxide nanomaterials is limited to the adsorption of one monolayer of heavy metal ions. Figs. 3a and 3c show a visible change in the morphology of the CoNP, with the formation of hierarchical structures over the cobalt nanoparticle-surface confirming that the Mn is superficially and physically adsorbed. In a second step, Mn ions continue to grow on the surface of the adsorbed Mn ions through a possible covalent bond between oxygen atom and Mn ions to form MnO structure, and a catalytic effect from the cobalt atoms on which Mn ions have been first adsorbed. The hierarchical microstructure visible in Figs. 3b and 3c, support such adsorption, followed by a growth process. The presence of competing ions will prevent or interfere with the adsorption process through a possible direct interaction with the surface of CoNP covered by hydroxyl groups, or with Mn atoms already adsorbed on the surface of CoNP, which is supported by the decrease of the adsorption capacity in the presence of competing ions.

The study highlighted that nanocobalt-based sand nanocomposite exhibits a higher efficiency for high concentration of heavy ions. In addition, the ions are extracted in the form of a solid coating with a thickness of a few μm, which should enable the future reclamation of the extracted manganese to promote a circular economy. However, the reclamation process needs to be further investigated.

4. Conclusion

The adsorption of manganese ions on Cobalt based nanomaterials was investigated in batch-mode and continuous mode. For batch studies, we observed a maximum of 17.86 mg/g adsorption capacity of CoNP. Additionally, the experimental data showed a good fit for the Freundlich

Table 4

Comparison of manganese ions adsorption capacity published in recent studies. Acronyms: DMAPAAQ + FeOOH: N,N′-Dimethylaminopropyl acrylamide, methyl chloride quaternary loaded with iron hydroxide, PSA-GO: Poly(sodium acrylate)-graphene oxide.

Adsorbent	Mn source	C_0 (mg/L)	Mass of adsorbent	Adsorption capacity (mg/g)	Mode of study	Model (s)	Ref
Graphene Oxide–ZnO Nano-composites	$MnSO_4 \cdot H_2O$	4.9–10.5	20 mg	5.6 (pH=5) 12.6 (pH=4)	Batch	Langmuir Freundlich Temkin	[33]
DMAPAAQ + FeOOH	$MnSO_4 \cdot 5 H_2O$	25	20 mg	39.02 (pH=7)	Batch	Langmuir	[34]
Fe-pumice composite	Mn (II)	20–100	500 mg	2.19 (pH=7)	Batch	Langmuir Freundlich Temkin	[35]
Sodium Alginate / Graphene Oxide Composite (Hydrogel)	$MnCl_2 \cdot 4 H_2O$	10–200	150 mg	56.49 (pH=6)	Batch	Langmuir Freundlich Temkin	[36]
(PSA–GO) double network hydrogel	$KMnO_4$	20–600	8 mg	165.5 (pH=6)	Batch	Langmuir Freundlich Temkin	[37]
Magnetic Graphene Oxide	$MnCl_2 \cdot 4 H_2O$	82.5	30 mg	15 (pH=5.5)	Batch	Langmuir Freundlich	[16]
Magnetic Nanocobalt	$KMnO_4$	0.1–100	10 mg	17.86	Batch	Langmuir Freundlich	Our study
Cobalt based sand nano-composite	$KMnO_4$	30–85	7.8 g	274.4 (30 mg/L) 584.5 (50 mg/L) 3360.3 (85 mg/L)	Flow	Thomas Yoon-Nelson	Our study

model indicating a multilayered adsorption of Mn ions and the low value could be attributed to nanoparticle agglomeration that cannot be avoided in aqueous solutions. The physical adsorption of Mn ions in solid form was confirmed by X-ray diffraction and SEM on exhausted CoNP investigated in batch-mode after adsorption. The dynamic-mode studies were conducted with different initial Mn concentrations, different pH ranging from 4 to 12, and in presence of competing ions (Fe^{3+}, Cu^{2+}, As^{3+} and As^{5+}). Thomas and Yoon-Nelson models were applied to determine the adsorption capacity and other parameters (i.e., Thomas model constant (K_{TH}), Yoon-Nelson model constant (K_{YN}), and time required for 50% adsorption (Ţ)). The filter performed best for higher concentrations, and at pH = 7, with an extraction capacity of 3360.3 mg/g. Similarly to batch-mode, the physical adsorption of Mn ions in solid form was also confirmed by FTIR study and X-ray tomography performed on exhausted CCS filter investigated in flow mode. In the presence of competing ions, we observed that the presence of ferric ions slightly decreases the adsorption capacity of manganese ions, which remain at 2974.1 mg/g. However, the presence of copper ions and arsenic ions compete in the adsorption process and lower Mn ion adsorption values were measured. It highlights that mCCS can also adsorb simultaneously other heavy metal ions through a competitive adsorption and can be used to treat water that contains multiple metallic pollutants. The extraction of these other metallic pollutants must be further studied. Thus, cobalt coated sand showed a great potential in extracting Mn ions from contaminated water even in the presence of other competing ions and can be a promising technology for the removal of toxic metallic ions from groundwater. The possible reclamation of the extracted pollutant from the exhausted mCCS needs to be further investigated.

CRediT authorship contribution statement

The manuscript was written through contributions of all authors. R. Kumar performed the water purification experiments, data treatment, and manuscript writing;P. Rauwel: contributed to background theory, methodology, experimental setup, data analysis, supervision, provided feedback and contributed to writing;M. Kriipsalu: contributed to data analysis, supervision and provided feedback;D. Wragg: contributed to XRD analyses and treatment;E. Rauwel: contributed to resources and funding acquisition, methodology, experiments, analysis, interpretation, identification of the phases, XRD treatment, test of extractions, mechanism of adsorption, supervision and manuscript correction and writing. All authors have given approval to the final version of the manuscript.

Declaration of Competing Interest

The authors declare that they have no known competing financial interests or personal relationships that could have appeared to influence the work reported in this paper.

Data Availability

Data will be made available on request.

Acknowledgements

Appendix A. Supporting information

Supplementary data associated with this article can be found in the online version at doi:10.1016/j.jece.2023.109818.

References

[1] P.B. Tchounwou, C.G. Yedjou, A.K. Patlolla, D.J. Sutton, Heavy metal toxicity and the environment, Exp. Suppl 101 (2012) 133–164.

[2] Y. Zhai, X. Cao, X. Xia, B. Wang, Y. Teng, X. Li, Elevated Fe and Mn concentrations in groundwater in the songnen plain, Northeast China, and the factors and mechanisms involved, Agronomy 11 (2021) 2392.

[3] A.M. Muliwa, T.Y. Leswifi, A. Maity, A. Ochieng, M.S. Onyango, Fixed-bed operation for manganese removal from water using chitosan/bentonite/MnO composite beads, Environ. Sci. Pollut. Res. Int. 25 (2018) 18081–18095.

[4] M. Aschner, K.E. Vrana, W. Zheng, Manganese uptake and distribution in the central nervous system (CNS), Neurotoxicology 20 (1999) 173–180.

[5] J. Crossgrove, W. Zheng, Manganese toxicity upon overexposure, NMR Biomed. 17 (2004) 544–553.

[6] U.S.E.P. Agency, Drinking Water Regulations and Contaminants, in, 2022.

[7] U.S.E.P. Agency, Contaminant Candidate List (CCL) and Regulatory Determination, in, 2022.

[8] R.M. Freitas, T.A.G. Perilli, A.C.Q. Ladeira, Oxidative precipitation of manganese from acid mine drainage by potassium permanganate, J. Chem. 2013 (2013), 287257.

[9] D.S. Patil, S.M. Chavan, J.U.K. Oubagaranadin, A review of technologies for manganese removal from wastewaters, J. Environ. Chem. Eng. 4 (2016) 468–487.

[10] D.A. white, A. Asfar-Siddique, Removal of manganese and iron from drinking water using hydrous manganese dioxide, Solvent Extr. Ion.-. Exch. 15 (1997) 1133–1145.

[11] V.A. Pacini, A. María Ingallinella, G. Sanguinetti, Removal of iron and manganese using biological roughing up flow filtration technology, Water Res 39 (2005) 4463–4475.

[12] A. Piazza, L. Ciancio Casalini, V.A. Pacini, G. Sanguinetti, J. Ottado, N. Gottig, Environmental bacteria involved in manganese(II) oxidation and removal from groundwater, Front. Microbiol. 10 (2019).

[13] N.R. Barboza, S.S. Amorim, P.A. Santos, F.D. Reis, M.M. Cordeiro, R. Guerra-Sá, V. A. Leão, Indirect manganese removal by stenotrophomonas sp. and Lysinibacillus sp. isolated from brazilian mine water, BioMed. Res. Int. 2015 (2015), 925972.

[14] A.-M. Gounot, Microbial oxidation and reduction of manganese: consequences in groundwater and applications, FEMS Microbiol. Rev. 14 (1994) 339–349.

[15] S.T. McBeath, D.P. Wilkinson, N.J.D. Graham, Advanced electrochemical oxidation for the simultaneous removal of manganese and generation of permanganate oxidant, Environ. Sci.: Water Res. Technol. 6 (2020) 2405–2415.

[16] H. Yan, H. Li, X. Tao, K. Li, H. Yang, A. Li, S. Xiao, R. Cheng, Rapid removal and separation of Iron(II) and Manganese(II) from micropolluted water using magnetic graphene oxide, ACS Appl. Mater. Interfaces 6 (2014) 9871–9880.

[17] P. Rauwel, E. Rauwel, Towards the extraction of radioactive cesium-137 from water via graphene/CNT and nanostructured prussian blue hybrid nanocomposites: a review, Nanomaterials 9 (2019) 682.

[18] P. Rauwel, W. Uhl, E. Rauwel, Editorial for the special issue on 'application and behavior of nanomaterials in water treatment', Nanomaterials 9 (2019) 880.

[19] R. Kumar, P. Rauwel, E. Rauwel, Nanoadsorbants for the removal of heavy metals from contaminated water: current scenario and future directions, Processes 9 (2021) 1379.

[20] K. Nakamoto, T. Kobayashi, Arsenate and arsenite adsorbents composed of nano-sized cerium oxide deposited on activated alumina, Sep. Sci. Technol. 54 (2019) 523–534.

[21] Z.Z. Chowdhury, S.M. Zain, A.K. Rashid, R.F. Rafique, K. Khalid, Breakthrough curve analysis for column dynamics sorption of Mn(II) ions from wastewater by using mangostana garcinia peel-based granular-activated, Carbon, J. Chem. 2013 (2013), 959761.

[22] K.A. Emmanuel, A.V. Rao, Comparative study on adsorption of Mn(II) from aqueous solutions on various activated carbons, E-J. Chem. 6 (2009), 587159.

[23] Y. Zhang, J. Zhao, Z. Jiang, D. Shan, Y. Lu, Biosorption of Fe(II) and Mn(II) ions from aqueous solution by rice husk ash, BioMed. Res. Int. 2014 (2014), 973095.

[24] A. Adeogun, E. Ofudje, M. Idowu, S. Kareem, Equilibrium, kinetic, and thermodynamic studies of the biosorption of Mn(II) ions from aqueous solution by raw and acid-treated corncob biomass, BioResources 6 (2011) 4117–4134.

[25] V. Rocher, J.M. Siaugue, V. Cabuil, A. Bee, Removal of organic dyes by magnetic alginate beads, Water Res 42 (2008) 1290–1298.

[26] E. Rauwel, S. Al-Arag, H. Salehi, C.O. Amorim, F. Cuisinier, M. Guha, M.S. Rosario, P. Rauwel, Assessing cobalt metal nanoparticles uptake by cancer cells using live raman spectroscopy, Int J. Nanomed. 15 (2020) 7051–7062.

[27] M.R. Pérez, I. Pavlovic, C. Barriga, J. Cornejo, M.C. Hermosín, M.A. Ulibarri, Uptake of Cu2+, Cd2+ and Pb2+ on Zn–Al layered double hydroxide intercalated with edta, Appl. Clay Sci. 32 (2006) 245–251.

[28] I. Zekker, E. Rikmann, T. Tenno, A. Menert, V. Lemmiksoo, A. Saluste, T. Tenno, M. Tomingas, Modification of nitrifying biofilm into nitritating one by combination

of increased free ammonia concentrations, lowered HRT and dissolved oxygen concentration, J. Environ. Sci. 23 (2011) 1113–1121.

[29] R.-C. Xie, C. Batchelor-McAuley, E. Rauwel, P. Rauwel, R.G. Compton, Electrochemical characterisation of Co@Co(OH)2 core-shell nanoparticles and their aggregation in solution, ChemElectroChem 7 (2020) 4259–4268.

[30] V. Manirethan, N. Gupta, R.M. Balakrishnan, K. Raval, Batch and continuous studies on the removal of heavy metals from aqueous solution using biosynthesised melanin-coated PVDF membranes, Environ. Sci. Pollut. Res 27 (2020) 24723–24737.

[31] X.Q. Zhao, S. Veintemillas-Verdaguer, O. Bomati-Miguel, M.P. Morales, H.B. Xu, Thermal history dependence of the crystal structure of Co fine particles, Phys. Rev. B 71 (2005), 024106.

[32] T. Ericsson, The temperature and concentration dependence of the stacking fault energy in the Co-Ni system, Acta Metall. 14 (1966) 853–865.

[33] E. Leiva, C. Tapia, C. Rodríguez, Removal of Mn(II) from acidic wastewaters using graphene Oxide–ZnO nanocomposites, Molecules 26 (2021) 2713.

[34] S.R. Safi, T. Gotoh, Simultaneous removal of arsenic and manganese from synthetic aqueous solutions using polymer gel composites, Nanomaterials 11 (2021) 1032.

[35] D.İ. Çifçi, S. Meriç, Manganese adsorption by iron impregnated pumice composite, Colloids Surf. A: Physicochem. Eng. Asp. 522 (2017) 279–286.

[36] X. Yang, T. Zhou, B. Ren, A. Hursthouse, Y. Zhang, Removal of Mn (II) by sodium alginate/graphene oxide composite double-network hydrogel beads from aqueous solutions, Sci. Rep. 8 (2018) 10717.

[37] R. Xu, G. Zhou, Y. Tang, L. Chu, C. Liu, Z. Zeng, S. Luo, New double network hydrogel adsorbent: highly efficient removal of Cd(II) and Mn(II) ions in aqueous solution, Chem. Eng. J. 275 (2015) 179–188.